Structural Engineering and Mechanics, Vol. 25, No. 3 (2007) 291-310
DOI: http://dx.doi.org/10.12989/sem.2007.25.3.291

Ground strain estimation for lifeline earthquake engineering

Takeshi Koike†, Osamu Maruyama‡, and Lessandro Estelito Garciano

Musashi Institute of Technology, 1-28-1 Tamazutsumi, Setagaya-ku, Tokyo, 158-8557, Japan

(Received February 9, 2005, Accepted February 5, 2006)

Abstract. Current seismic design guidelines in Japan are diverse in the seismic ground strain estimates, because the concepts on a horizontally propagating wave model are not consistent in various seismic design guidelines including gas, water and other underground structures. The purpose of this study is (a) to derive the analytical methods to estimate the ground strains for incident seismic waves, (b) to develop a statistical estimation technique of the ground strains, and finally (c) to compare the theoretical estimation with the observed data which was measured at 441 sites in the 1999 Chi-Chi Earthquake in Taiwan.

Keywords: ground strain; spatial variation; buried pipelines; seismic waves.

1. Introduction

For all the underground pipelines, the structural (pipe) strain is converted from the free field ground strain by means of a conversion factor (Ogawa *et al.* 2001) which depends on the geometry of the buried pipe. In fact, the tasks of evaluating the free field ground strain and estimating the pipe strain are of crucial importance for a seismic risk analysis of an underground pipeline system; especially when the analysis must provide risk information that is realistic and useful in engineering design.

Current seismic design guidelines in Japan are diverse in the free field ground strain estimates, because the concepts on a horizontally propagating wave model are not consistent in various seismic design guidelines including gas, water and other underground structures. In fact, a seismic wave model with a longitudinal amplitude along the surface layer is used in the seismic design guideline of gas pipelines (JGA 2000), while water pipeline (JWWA 1998) and other buried pipeline structures are designed on the basis of such a wave with its transverse amplitude equal to the seismic response by an incident SH ground motion. The horizontally propagating wave velocity, however, is different among those pipeline systems. The gas pipeline, for instance, adopts the phase velocity at a typical frequency of the specific site which is given by the dispersion characteristics of the Rayleigh type surface wave. Other pipelines use the wave velocity given by the harmonic mean value of the shear wave velocities of a layered medium resting on a firm rock formation, although

† Professor, Corresponding author, E-mail: tkoike@sc.musashi-tech.ac.jp
‡ Associate Professor, E-mail: omaruya@sc.musashi-tech.ac.jp

its physical meanings are not clear.

Why is such a fictitious wave model based on SH wave utilized in the current design guidelines? One main reason comes from the belief that actual pipe damages are not produced by surface waves, but by body waves. If a body wave model is valid for estimating the ground strain for buried pipelines, this fictitious wave must have a spatial variation along the horizontal direction. This spatial variation can be given by phase delay of incident wave propagating in the firm rock formation, or by spatial inhomogenity (Loh 1988, Hong *et al.* 1999, Di Paola *et al.* 2000) in soil properties in the layered medium.

In the present study, therefore, emphasis is placed on a more accurate evaluation of the free field ground strain by improving the current methods. The free field ground strain ε_G can be estimated as $\varepsilon_G = \dot{u}_{\max}/V$ in which $\dot{u}_{\max}$ = peak ground velocity; and V = phase velocity of the seismic wave propagating at a typical frequency. There are several different definitions, however, on the propagating seismic wave velocity which are estimated from (1) baserock shear wave model, (2) apparent shear wave model combining baserock wave propagation with an effect of spatial variation in soil properties in the surface layered medium, (3) Rayleigh type surface wave, and (4) Love type surface wave.

It is recognized that a seismic wave consists of a spectrum of randomly phased frequency components. The ground strain and motions are, therefore, modeled as stationary Gaussian processes. A known solution for a boundary value problem involving the surface wave and a ground model as described above has been used to find the ground strain and motion processes. The ground acceleration at the ground surface is also modeled as a stationary Gaussian process with a specified spectral density, and is used as one of the boundary conditions. The non-stationarity of the ground motion is accounted for by truncating these processes before time $t = 0$, and after $t = T$ where T = the duration of the ground motion.

Ground strain by the theoretical approach can be compared with that by the field observation approach. In the 1999 Chi-Chi Earthquake, spatially distributed ground motion were observed at 441 measurement points to be prepared by Central Weather Bureau (CWB) of Taiwan (Lee 2001). Using these acceleration data, the particle velocity, ground strain and phase velocity over the Taiwan island are analyzed and compared with the theoretical results.

2. Seismic design method of buried pipelines

2.1 Simplified ground strain estimate in current design guidelines

A buried pipe is deformed with a surrounding ground motion. So the current seismic design for the buried pipeline has been established with furnishing the simplified design formula of the ground deformation, the ground strain and the pipe strain.

The formula to estimate the ground deformation is derived hereunder.

Now we consider a long straight pipeline embedded in an infinite and homogeneous medium which is excited by a traveling seismic wave with certain incident angle to the pipe axis as shown in Fig. 1. When a seismic wave arrives at the baserock, the surface ground is amplified in accordance with the periodic response characteristics. Based on the seismic analysis of one-dimensional wave propagation in the elastic soil medium with a shear velocity of V_S, the free field displacement U_h can be given by

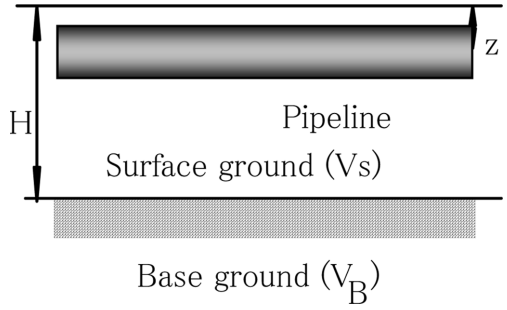

Fig. 1 Schematic example of the surface ground and buried pipeline

$$U_h = \frac{2}{\pi^2} S_V T_G \cos\left(\frac{\pi}{2H} z\right) \tag{1}$$

where S_V is the response (velocity) spectrum of the incident earthquake, H is the thickness of the surface ground, z is the soil depth to the pipe center, and T_G is the typical period of the surface ground which is defined by $T_G = 4H/V_S$.

Once the ground displacement is obtained, the simplified formula of the maximum ground strain is formulated, based on the following discussion.

The motion of the soil particle depends on the type of waves, but can always be resolved into a longitudinal component and a transverse component relative along the wave propagating axis. In general, two types of surface waves, Rayleigh wave and Love wave, correspond to those wave components, while the shear wave propagating from the focal area can also produce a longitudinal motion along the surface ground which is resulting from the phase delay effect. It can be noted, however, that there are not any generally accepted method to define the wave velocity traveling horizontally in the surface ground.

Assuming that the sinusoidal wave motion propagates in the horizontal direction, the free field strain ε_G is given by differentiation with respect to the horizontal component in the following way.

$$\varepsilon_G = \frac{2\pi}{L} U_h \tag{2}$$

where L is a wave length in the horizontal stretch.

2.2 Pipe strain formula

The current studies of seismic response of buried pipelines are usually based on the simplified model of a straight pipe embedded in an infinitive elastic (soil) medium for which the familiar differential equation can be established invoking D'Alembert's principle with respect to the inertia force, the internal force within the pipe and force proportional to the displacement u of the pipe relative to that of the free field u_G.

The equation for equilibrium of force in the direction longitudinal to the pipe axis is given by

$$\rho A \frac{\partial^2 u}{\partial t^2} - EA \frac{\partial^2 u}{\partial x^2} = K_1 (u_G - u) \tag{3}$$

in which u is pipe displacement in the longitudinal components; u_G is apparent free field displacement in the longitudinal component; ρ and E are mass density and Young's modulus of the pipe material; A is the cross-sectional area of the pipe; K_1 is the equivalent spring modulus to reflect the soil-structure interaction in the longitudinal direction.

Ignoring the inertia effect for the buried pipeline, the analytical result from Eq. (3) furnishes the pipe strain with the conversion factor α_0 as the ratio of the pipe displacement to the free field displacement in the same direction:

$$\varepsilon_s = \alpha_0 \varepsilon_G \tag{4}$$

in which

$$\alpha_0 = \frac{1}{1 + \left(\frac{2\pi}{\lambda \cdot L_a}\right)^2}, \qquad \lambda = \sqrt{\frac{K_1}{EA}} \tag{5}$$

where L_a = the apparent traveling wave length along the pipe axis.

2.3 Current design methods in Japan

2.3.1 Design guideline of Japan Gas Association (JGA 2000)

When a seismic wave excites a buried gas pipeline, a pipe strain is controlled by a longitudinal component much larger than a vertical one. So the seismic wave is modeled with a longitudinal amplitude along the surface layer in the design guideline of Japan Gas Association. This wave model is similar to Rayleigh wave type ground motion, the vertical component of which is neglected in JGA. And also JGA introduced the phase velocity in order to estimate the ground strain.

Based on the above discussion, the pipe strain ε_p is calculated with a longitudinal ground strain ε_G^{JGA} and a conversion factor α_0 of Eq. (5) in the following way.

$$\varepsilon_p = \alpha_0 \varepsilon_G^{JGA} \tag{6}$$

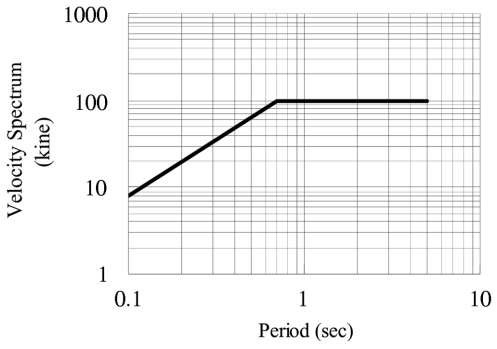

Fig. 2 Velocity spectrum used in JGA

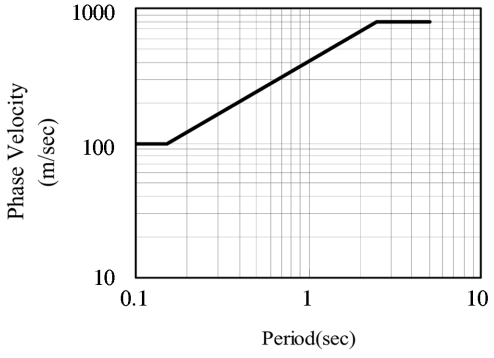

Fig. 3 Phase velocity curve used in JGA

in which

$$\varepsilon_G^{JGA} = \frac{4}{\pi}\frac{S_V}{V^{JGA}} \tag{7}$$

The velocity spectrum S_V and the phase velocity V^{JGA} for the typical period T_G of the surface ground are given by Figs. 2 and 3. The phase velocity of JGA guideline is the lower envelope of the analytical results of the dispersion curve for the Rayleigh wave type ground motion. One may understand that the upper value of 800 m/sec in Fig. 3 is fixed for the design purpose to provide the larger strain in the surface ground of a longer typical period.

2.3.2 Design guideline of Japan Water Works Association (JWWA 1998)

A water pipeline and other buried underground structures in Japan adopted a wave model with its transverse amplitude equal to the seismic response by an incident SH ground motion. This design model was based on the conviction that the ground strain generated by a body wave can contribute to the pipe failure, but the ground strain by a surface wave cannot achieve the failure event.

Based on the these discussion, the pipe strain ε_p is calculated with a longitudinal component of the ground strain ε_G^{JWWA} from an amplitude of SH wave ground motion and a conversion factor α_0 of Eq. (5) in the following way.

$$\varepsilon_p = \alpha_0 \varepsilon_G^{JWWA} \tag{8}$$

in which

$$\varepsilon_G^{JWWA} = \frac{4}{\pi}\frac{S_V}{V^{JWWA}} \tag{9}$$

Since the horizontally propagating velocity V^{JWWA} for the typical period T_G of the surface ground does not have any dispersion characteristics because of a body wave concept, the velocity is calculated with a simplified formula as follows:

$$V^{JWWA} = \frac{2V_S V_B}{V_S + V_B} \tag{10}$$

3. Ground strain estimation based on the wave models with power spectral contents

3.1 Ground model

Consider $n-1$ parallel, homogeneous and isotropic soil layers resting on a semi-infinite rock formation (basement layer) as shown in Fig. 1. Shown also in this figure is the seismic wave propagating in the horizontal direction and the underground pipeline buried in the first layer at a depth, z_1. The surface wave produces a horizontal ground surface acceleration, $\ddot{u}_s(t)$, in the direction of wave propagation which can be expressed under the assumption of a stationary stochastic process in the following form:

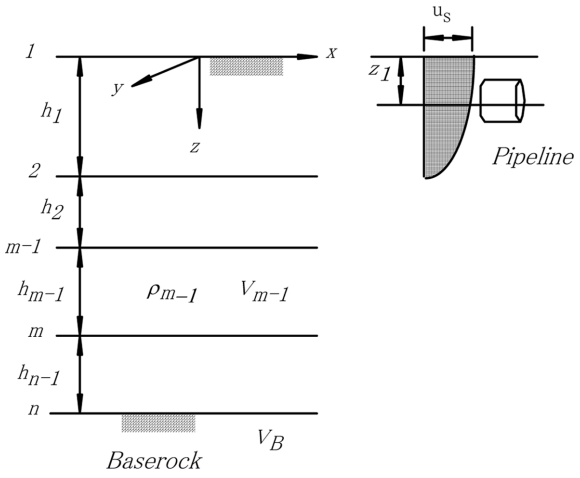

Fig. 4 Multi-layered model for ground

$$\ddot{u}_s(t) = \sum_{j=1}^{N} \sqrt{2G_{\ddot{u}_s}(\omega_j)\Delta\omega}\exp[i(\omega_j t + \phi_j)] \tag{11}$$

in which $G_X(\omega_j)$ = one-sided power spectral density of a stationary random process denoted by $X = X(t)$; $\omega_j = j\Delta\omega$, $\Delta\omega = \omega_u/N$; ϕ_j = independent random phase angles distributed over 0 to 2π and N = number of superposed harmonic components.

3.2 Ground strains based on various definitions of wave velocities

When an incident SH wave arrives with a delay proportional to the horizontally propagating duration in the baserock ground with the shear wave velocity V_B, the ground response at the surface layer appears with the same delay in the x direction of Fig. 1, so that the SH wave seems to travel horizontally with a velocity less than the baserock velocity. Although this SH wave does not arrive exactly with a horizontal travel delay of V_B, it can be assumed for our practical purpose that this velocity is approximately V_B. If there is a spatial variation in the soil rigidity of the surface layer in the horizontal direction, the seismic response produces not only ground response due to a phase delay of the incident SH wave but also an additional ground response due to spatial variation of soil rigidity.

3.3 SH wave propagating with baserock shear velocity

In the case of a delay due to an incident SH wave arrival without any spatial variation, the ground response displacement is given in the following form;

$$u_B(t) = \sum_{j=1}^{N} \sqrt{2G_{\ddot{u}_s}(\omega_j)\Delta\omega}\left|H^B(\omega_j)\right|/(i\omega_j)^2\exp[i(\omega_j t - k_B x + \phi_j)] \tag{12}$$

in which k_1 and k_B are the wave numbers of the first layer and baserock of the surface ground,

respectively, while, if the surface ground can be approximately expressed by a single layer model with the equivalent shear velocity $\overline{V}_1$, the frequency transmission function H^B for the surface ground is simply given by

$$\left|H^B(\omega_j)\right| = \cos\{k_1(\omega_j)z_1\} \quad \text{and} \quad k_B = \frac{\omega_j}{V_B}, \quad k_1(\omega_j) = \frac{\omega_j}{\overline{V}_1} \tag{13}$$

with the mean value $\overline{V}_1$ of shear velocity at the first layer.

Differentiating Eq. (12) with respect to x, the axial ground strain ε_G in the direction of wave propagation is obtained as;

$$\varepsilon_G(t) = \sum_{j=1}^{N} \sqrt{2G_\varepsilon^B(\omega_j)\Delta\omega}\exp[i(\omega_j t - k_B x + \phi_j)] \tag{14}$$

with

$$G_\varepsilon^B(\omega_j) = G_{\ddot{u}_s}(\omega_j)\cdot(k_B/\omega_j^2)^2\left|H^B(\omega_j)\right|^2 \tag{15}$$

3.4 SH wave with spatial variation of soil rigidity in the surface layer

When the effect of spatial variation is taken into consideration, the ground response is evaluated with two components due to a delay arrival and due to a spatial variation. A spatial variation of soil rigidity of the first layer along the horizontal direction can be modeled with the mean value of shear velocity $\overline{V}_1$ and its variation $v(x)$ in the following way;

$$V_1(x) = \overline{V}_1(x) + v(x) \tag{16}$$

with the variation of shear velocity to be modeled as

$$v(x) = \sqrt{2}\sum_{j=1}^{N} \sqrt{2S_v(\kappa_j)\Delta\kappa}\cos(\kappa_j x + \psi_j) \tag{17}$$

in which the stochastic property of the shear velocity variation is expressed with the stationary two-sided spectral density function $S_v(\kappa)$ with its wave number κ and phase angle ψ. When the autocorrelation of v is assumed with the standard deviation σ_{V1} and specific distance b;

$$R_v(x_1, x_2) = \sigma_{V_1}^2 \exp\left(-\frac{|x_1 - x_2|}{b}\right) \tag{18}$$

The corresponding spectral density is calculated in the following way:

$$S_v(\kappa) = 2\sigma_{V_1}^2 \frac{b}{1 + b^2\kappa^2} \tag{19}$$

Then the ground responses have similar expressions with Eqs. (12) to (15) under the spatial variation along the horizontal component denoted by x;

$$u_{SH}(t) = \sum_{j=1}^{N} \sqrt{2G_{\ddot{u}_s}(\omega_j)\Delta\omega}\left|H^{SH}(\omega_j, x)\right|/(i\omega_j)^2 \exp[i(\omega_j t - k_B x + \phi_j)]$$

$$\varepsilon_{SH}(t) = \sum_{j=1}^{N} \sqrt{2G_{\varepsilon}^{SH}(\omega_j)\Delta\omega}\exp[i(\omega_j t - k_B x + \phi_j)] \tag{20}$$

$$G_{\varepsilon}^{SH}(\omega_j) = G_{\ddot{u}_s}(\omega_j)\cdot(k_B/\omega_j^2)^2\left|H^{SH}(\omega_j, x)\right|^2$$

Since the function $H_{SH}(\omega_j, x)$ has two components of wave response and spatial variation, their combined expression is given as follows:

$$\left|H^{SH}(\omega_j, x)\right|^2 = \left|H^{SH}(\omega_j)\right|^2\left\{\frac{\left|H^{SH}(\omega_j|V_1(x))\right|^2}{\left|H^{SH}(\omega_j)\right|^2} + \left[\frac{\partial H^{SH}(\omega_j|V_1(x))}{\partial x}\right]^2\cdot\frac{1}{(k_B^2)\left|H^{SH}(\omega_j)\right|^2}\right\} \tag{21}$$

An approximation of Eq. (21) is carried out with the assumption that the first term of the bracket is approximately equal to be the unity, while, noting that $\partial H^{SH}/\partial x = \partial H^{SH}/\partial V_1 \cdot \partial V_1/\partial x$, the second term is given by the expectation of $\partial H^{SH}/\partial V_1$ times the expectation of the maximum value $(\partial V_1/\partial x)_{\max}$ of a stationary random process $V(x)$ of Eq. (16). If one may assume the random value of $\partial V_1/\partial x$ has Rayleigh distribution, the expectation of the extreme value of $\partial V_1/\partial x$ has an analytical solution with its standard deviation. Then Eq. (21) is expressed in the following way.

$$\left|H^{SH}(\omega_j, x)\right|^2 \approx \left|H^{SH}(\omega_j)\right|^2\left\{1 + \frac{\left[\left|E\left[\frac{\partial H^{SH}(\omega_j|V_1(x))}{\partial V_1}\right]\right|\cdot\left(\sqrt{2\ln n} + \frac{0.577215}{\sqrt{2\ln n}}\right)\sqrt{E\left[\left|\frac{\partial V_1}{\partial x}\right|^2\right]}\right]^2}{(k_B^2)\left|H^{SH}(\omega_j)\right|^2}\right\} \tag{22}$$

in which n is the sample size to be equal to the duration in second of the earthquake ground motion, and

$$\sqrt{E\left[\left|\frac{\partial V_1}{\partial x}\right|^2\right]} = \sqrt{\sum_{j=1}^{N}(\kappa_j)^2\cdot 4S_v(\kappa_j)\Delta\kappa}, \quad H^{SH}\{\omega_j|V_1(x)\} = \cos\{k_1(\omega_j;x)z_1\},$$

$$k_1(\omega_j;x) = \frac{\omega_j}{V_1(x)} \tag{23}$$

3.5 Surface models

The surface wave produces a horizontal ground motion in the direction of wave propagation, in which Rayleigh wave type and Love wave type models are adopted as a typical surface wave model for a simplified version of seismic design guidelines for buried pipelines. Especially, Love wave type model, which can produce a transverse component in the direction of wave propagation, is a comparative model with the SH wave model described in the previous section.

3.6 Rayleigh wave type model

According to Haskell (1953), the ground response and its normal strain for Rayleigh wave type model are given in Eq. (24) with the phase velocity $V_R(\omega)$ obtained from the dispersion curve of the surface ground of Fig. 4.

$$\begin{aligned} u_R(t) &= \sum_{j=1}^{N} \sqrt{2G_{\ddot{u}_s}(\omega_j)\Delta\omega}\left|H^R(\omega_j)\right|/(i\omega_j)^2 \exp[i(\omega_j t - k_R x + \phi_j)] \\ \varepsilon_R(t) &= \sum_{j=1}^{N} \sqrt{2G_{\varepsilon}^R(\omega_j)\Delta\omega}\exp[i(\omega_j t - k_R x + \phi_j)] \\ G_{\varepsilon}^R(\omega_j) &= G_{\ddot{u}_s}(\omega_j)\cdot(k_R/\omega_j^2)^2\left|H^R(\omega_j)\right|^2 \end{aligned} \tag{24}$$

in which k_R is the wave number of Rayleigh wave to be given by the dispersion curve $V_R(\omega)$, and the detail expression of $H_R(\omega)$ was developed by Shinozuka *et al.* (1983).

$$k_R = \frac{\omega_j}{V_R(\omega_j)}, \quad \left|H^R(\omega_j)\right| = \{S_{m11}(z_m) + \eta S_{m12}(z_m)\}, \quad \eta = \frac{\dot{w}_0}{\dot{u}_0} \tag{25}$$

where $S_{m11}(z_m)$ and $S_{m12}(z_m)$ are given in the Appendix.

3.7 Love wave type model

The similar approach can be taken to obtain the ground response and its strain for Love wave type model as follows:

$$\begin{aligned} u_L(t) &= \sum_{j=1}^{N} \sqrt{2G_{\ddot{u}_s}(\omega_j)\Delta\omega}\left|H^L(\omega_j)\right|/(i\omega_j)^2 \exp[i(\omega_j t - k_L x + \phi_j)] \\ \varepsilon_L(t) &= \sum_{j=1}^{N} \sqrt{2G_{\varepsilon}^L(\omega_j)\Delta\omega}\exp[i(\omega_j t - k_L x + \phi_j)] \\ G_{\varepsilon}^L(\omega_j) &= G_{\ddot{u}_s}(\omega_j)\cdot(k_L/\omega_j^2)^2\left|H^L(\omega_j)\right|^2 \end{aligned} \tag{26}$$

in which k_L is the wave number of Love wave to be given by the dispersion curve $V_L(\omega)$,

$$k_L = \frac{\omega_j}{V_L(\omega_j)} \tag{27}$$

and the amplification factor (Kramer 1996) is derived from those equations hereunder.

$$\begin{aligned} \left|H^L(\omega_j)\right| &= P_k\cos\{\tilde{\beta}_k(\omega_j)z_k\} + Q_k\sin\{\tilde{\beta}_k(\omega_j)z_k\} \\ V > V_k \qquad \tilde{\beta}_k(\omega_j) &= \sqrt{\left(\frac{V}{V_k}\right)^2 - 1}\cdot\frac{\omega_j}{V} \end{aligned} \tag{28}$$

$$V \le V_k \qquad \tilde{\beta}_k(\omega_j) = \sqrt{1 - \left(\frac{V}{V_k}\right)^2} \cdot \frac{\omega_j}{V}$$

$$\begin{pmatrix} P_k \\ Q_k \end{pmatrix} = \begin{bmatrix} \cos\{\tilde{\beta}_{k-1}(\omega_j)h_{k-1}\} & \sin\{\tilde{\beta}_{k-1}(\omega_j)h_{k-1}\} \\ -\mu_{k-1}\tilde{\beta}_{k-1}(\omega_j)\sin\{\tilde{\beta}_{k-1}(\omega_j)h_{k-1}\} & \mu_{k-1}\tilde{\beta}_{k-1}(\omega_j)\cos\{\tilde{\beta}_{k-1}(\omega_j)h_{k-1}\} \end{bmatrix} \begin{pmatrix} P_{k-1} \\ Q_{k-1} \end{pmatrix}$$

$$\mu_k = \rho_k V_k^2$$

3.8 Model of input ground motion

The incident seismic ground motion arrives at a rock formation in the layered medium, in which the ground surface acceleration $\ddot{u}_o(t)$ defined in Eq. (29) is constructed on the basis of fault parameters including the fault size, moment magnitude, corner frequency and any other site parameters.

$$\ddot{u}_o(t) = \sum_{j=1}^{N} \sqrt{2G_{\ddot{u}_0}(\omega_j)\Delta\omega}\exp[i(\omega_j t + \phi_j)] \tag{29}$$

in which the power spectral density $G_{\ddot{u}_0}(\omega)$ developed by Irikura (1986) is defined as

$$G_{\ddot{u}_0}(\omega) = CA_s(\omega)A_D(\omega)A_A(\omega) \tag{30}$$

where C, A_S, A_D, A_A are the radiation characteristic coefficient, the source spectrum proposed by Brune (1970), the damping characteristics of seismic wave traveling from the source and the local site amplification factor from the baserock to the ground surface, respectively. All the site parameters in these functions used hereunder are taken from the study of Harada (1995). Those parameters are given in the following expressions.

For the radiation characteristic coefficient,

$$C = \frac{R(\theta, \varphi)FV}{4\pi\rho C_s^3} \tag{31}$$

in which $R(\theta, \varphi)$, ρ, C_s, F, V are radiation directivity characteristics for shear waves (0.63), mass density (2.7 gr/cm^3), shear velocity (3.6 km/sec) and frequency correction at free surface (2.0) and reduction ratio (0.5) where the energy distribution is considered for two horizontal directions.

Kamae *et al.* (1991) discussed about numerical estimation of the source spectrum and its related parameters which are used for its numerical calculations in this study.

For the source spectrum,

$$A_s(\omega) = \frac{M_o\omega^2}{1 + \left(\frac{\omega}{\omega_c}\right)^2} \tag{32}$$

in which M_o, ω, ω_c are the earthquake moment (dyne-cm), frequency (radian) and corner frequency. The earthquake moment and the corner frequency by the Brune's relation are furnished as

$$M_o = 10^{(1.33M + 17.0)}, \qquad \omega_c = 2\pi \times 4.9 \times 10^6 C_s \left(\frac{\Delta\sigma}{M_o}\right)^{1/3} \tag{33}$$

where M is a magnitude the small earthquake, $\Delta\sigma$ is stress drop parameter in bar.

For the damping characteristics,

$$A_D(\omega) = \frac{1}{1 + (\omega/\omega_{\max})^n} \frac{1}{R} \exp\left(-\frac{\omega R}{2QC_s}\right) \tag{34}$$

in which $\omega_{\max}$, Q, R are the high frequency limit of a small earthquake, and the effects of geometrical damping and of material internal damping, respectively. $\omega_{\max}$ is simply given by

$$\omega_{\max} = 2\pi \times 10^{(1.82 - 0.160M)} \tag{35}$$

For the amplification factor, the Kanai-Tajimi model is introduced herein;

$$A_A(\omega) = \frac{\sqrt{1 + 4h_g^2\left(\frac{\omega}{\omega_g}\right)^2}}{\sqrt{\left\{1 - \left(\frac{\omega}{\omega_g}\right)^2\right\}^2 + 4h_g^2\left(\frac{\omega}{\omega_g}\right)^2}} \tag{36}$$

in which ω_g, h_g are the typical frequency of the surface ground and the parameter to control the amplification of ground response, respectively. The following values are adopted for various site conditions: $\omega_g = 15.6$ (rad/s), $h_g = 0.6$ for hard ground, $\omega_g = 10.68$ (rad/s), $h_g = 0.4$ for intermediate ground, and $\omega_g = 6.28$ (rad/s), $h_g = 0.2$ for soft ground.

The duration (Izumi 1994) T in which an earthquake accelerogram is greater than 10% of the maximum amplitude is evaluated with a magnitude M as follows;

$$T = 10^{\frac{(M-2.5)}{3.23}} \tag{37}$$

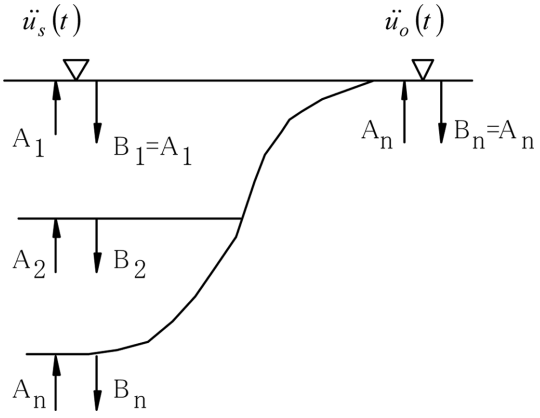

Fig. 5 The incident ground motion at the layered medium

3.9 Ground response at the ground surface

The ground motion $\ddot{u}_s(t)$ at the ground surface shown in Fig. 5 is propagated from an incident seismic wave. The power spectral density $G_s(\omega)$ is also calculated from

$$G_{\ddot{u}_S}(\omega_j) = \left|H_{n1}(\omega_j)\right|^2 G_{\ddot{u}_0}(\omega_j) \tag{38}$$

and

$$\left|H_{n1}(\omega_j)\right| = \frac{A_1}{A_n} \tag{39}$$

3.10 Maximum of free field strain

Since the ground strain is idealized as a stationary Gaussian process, its absolute maximum in the duration T, $\varepsilon_{\max} = \max_{0<t<T}|\varepsilon_G(t)| < \alpha$ is a random variable. Thus, the distribution function $F_\varepsilon(\alpha; T)$ of $\varepsilon_{\max}$ and the distribution function $F_{T0}(T\ ;\ \alpha)$ of the first passage time T_0 must be considered first. Writing $P(E)$ for the probability of event E, these distribution functions are defined as

$$F_{\varepsilon_{\max}}(\alpha;T) = P\{\max_{0\le t\le T}\left|\varepsilon_G(t,x)\right| \le \alpha\} = 1 - F_{T_0}(T;\alpha) \tag{40}$$

and

$$F_{T_0}(T;\alpha) = P\{T_0 \le T; \left|\varepsilon_G(T_0,x)\right| > \alpha\} \tag{41}$$

Using Vanmarcke's (1972) approximation method, Eq. (40) results in

$$F_{\varepsilon_{\max}}(\alpha;T) = erf\left(\frac{\alpha_0}{\sqrt{2}}\right)\exp\left\{-2\,\hat{\nu}_0 T\exp\left(-\frac{\alpha_0^2}{2}\right)\frac{1-\exp\left(-\frac{\sqrt{\pi}\hat{q}\,\alpha_0}{\sqrt{2}}\right)}{1-\exp\left(-\frac{\alpha_0^2}{2}\right)}\right\} \tag{42}$$

in which $erf(\ )$ indicates the error function and

$$\alpha_0 = \frac{\alpha}{\hat{\sigma}_\varepsilon},\quad \hat{\sigma}_\varepsilon = \sqrt{\hat{\lambda}_0},\quad \hat{q} = \sqrt{1-\frac{\hat{\lambda}_1}{\hat{\lambda}_0\hat{\lambda}_2}},\quad \hat{\nu}_0 = \frac{1}{2\pi}\sqrt{\frac{\hat{\lambda}_2}{\hat{\lambda}_0}}$$
$$\hat{\lambda}_i = \int_0^\infty \omega^i G_{\varepsilon_G}(\omega)d\omega,\qquad i = 0,1,2 \tag{43}$$

The expected value $E\{\varepsilon_{\max}\}$ and variance $Var\{\varepsilon_{\max}\}$ of $\varepsilon_{\max}$ are obtained from

$$E\{\varepsilon_{\max}\} = \int_0^\infty\{1 - F_{\varepsilon_{\max}}(\alpha;T)\}d\alpha$$
$$Var\{\varepsilon_{\max}\} = 2\int_0^\infty \alpha\{1 - F_{\varepsilon_{\max}}(\alpha;T)\}d\alpha - [E\{\varepsilon_{\max}\}] \tag{44}$$

Table 1 Ground surface models having various typical periods

Layer thickness	unit	Typical period (sec)								
		0.15	0.2	0.3	0.4	0.5	0.6	0.7	0.8	1
h_1	*m*	5	3.5	5.1	6.75	8.5	16.6	23.1	28.6	30
h_2	*m*	5	16.5	24.9	33.3	41.5	33.4	26.9	21.4	50

Layer thickness	unit	Typical period (sec)						Mass	Shear velocity
		1.3	1.5	2	3	4	5	ton/m^3	m/sec
h_1	*m*	40	52	80	105	127	182	1.7	80
h_2	*m*	60	48	20	95	174	118	2.2	300
Baserock								2.3	800

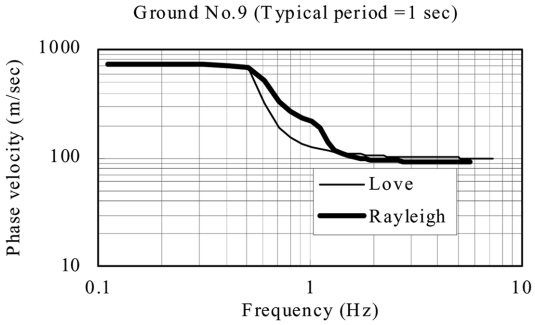

Fig. 6 The phase velocities of the model ground

4. Numerical examples

4.1 Ground models and soil conditions

A simple ground model with three layers is adopted in this numerical study. Ground surface models having different thicknesses are shown in Table 1.

Soil properties, mass and shear velocity have the same values for each layer. The shear velocity of the baserock is assumed to be 800 m/s which is consistent with the value used in the design guideline of Japan Gas Association.

4.2 Phase velocities

Dispersion curves for Rayleigh and Love waves are calculated for the ground models in Table 1. Fig. 6 is a schematic illustration of phase velocities of the model ground having the typical period of 1 second. This figure shows that the phase velocity in lower frequency approaches the shear velocity of baserock, while that in higher frequency reaches the shear velocity of the surface ground. These trends are valid for both wave models, although Rayleigh wave has a larger value of phase velocity in the range of 0.5 to 1.3 Hz.

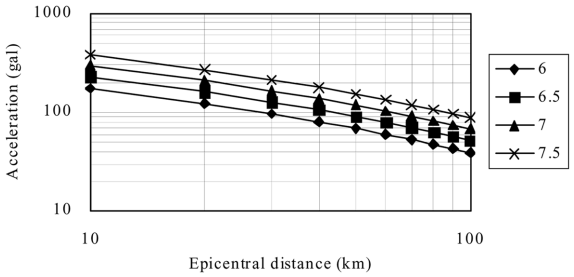

Fig. 7 Attenuation relationship of ground acceleration for various magnitudes of medium size of earthquakes

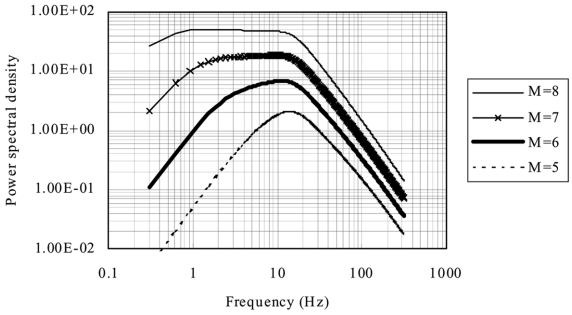

Fig. 8 The power spectral densities for various magnitudes

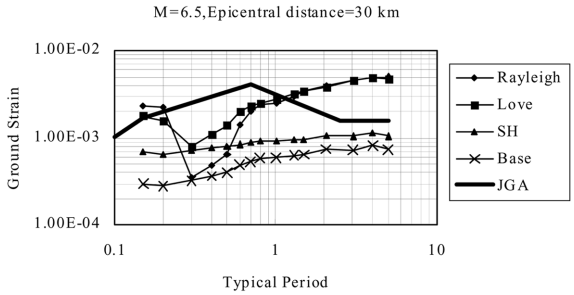

Fig. 9 Ground strains for various wave propagation models (Case1: Magnitude 6.5, epicentral distance 30 km)

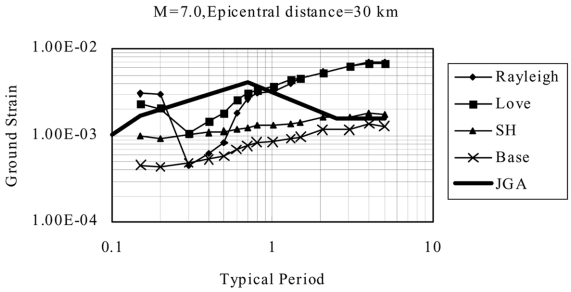

Fig. 10 Ground strains for various wave propagation models (Case2: Magnitude 7.0, epicentral distance 30 km)

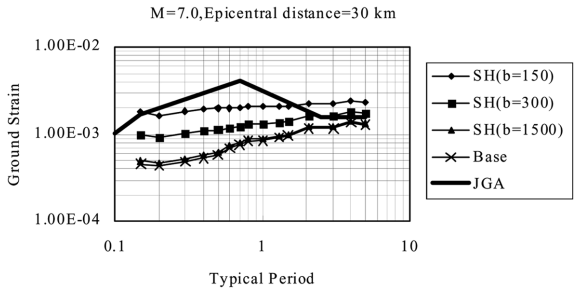

Fig. 11 Ground strain for SH wave with spatial variations

4.3 Input earthquake motion

A minimum size of ground motion is assumed herein. Attenuation property and Spectral density are specified by the stationary power spectral density of Eq. (30).

Fig. 7 shows the attenuation characteristics of input earthquake model adopted herein.

Fig. 8 is the power spectral densities for various magnitudes. It should be noted that larger magnitude can provide relatively greater spectral amplitude in a wider frequency range.

Figs. 9 and 10 show ground strains for various surface ground models when an earthquake occurs with the magnitude of 6.5 (Case 1) and that of 7.0 (Case 2) for the same epicentral distance of 30 km. In these figures, ground strains are calculated with Eq. (24) for Rayleigh wave model, Eq. (26) for Love wave model, Eq. (20) for SH wave model with spatial variations and Eq. (14) for seismic wave propagating in the baserock, respectively, while a thick line denoted by JGA is a design curve given in the seismic design guideline of Japan Gas Association. Both figures appear that the strain amplitude of surface waves provide larger than those of SH waves. JGA design curve is almost greater than strains given by SH wave models, while the surface wave models exceed the design curve in the range more than the typical period of 1 second. The lowest ground strain, located around the typical period of 0.3 second for the surface wave models, is a result of the characteristics of the dispersion curves shown in Fig. 6.

Current study shows that the structural strain of straight pipe is almost equal to the ground strain in the range greater than the typical period of 1.0 second, because any slippage effect cannot be expected in such a long wave length. This observation in Figs. 9 and 10 means that, if the ground strain is generated by surface waves, the ground strain may produce comparatively large pipe strain in the surface soft ground with a typical period of more than 1.0 second.

In Fig. 11, the effect of spatial variation is investigated, in which a short relative distance ($b = 150$ m) meaning heavier randomness within the short distance can produce larger strain than that in a longer separation distance ($b = 1500$ m).

5. Ground strain estimation based on the observation data

5.1 Spatial allocation of ground motion observation sites in the 1999 Chi-Chi Earthquake in Taiwan

Spatially distributed ground motion are observed at 441 measurement points to be prepared by Central Weather Bureau (CWB) of Taiwan. The digital strong motion records in the 1991 Chi-Chi Earthquake were prepared and processed by Lee *et al.* (2001). In this study those data are analyzed to estimate the phase velocity at the ground surface located near the fault zone of this earthquake.

The black dots in Fig. 13 show the locations of the observation sites in Taiwan. These sites are mainly distributed in the western part of Taiwan and are not equally spaced. The most dense allocation of the sites is less than 1 km apart from each other, but the other points are far from more than 5 km.

5.2 Ground strain estimate from observation data

The numerical analyses of the digital accelerograph records are developed in order to obtain the particle velocity, the ground strain and the phase velocity over the spatially extended area near the fault zone. The 1 km × 1 km meshes covers the whole area of Taiwan. Four grids of each mesh are estimation points of the ground responses. Since the measurement records are obtained at 441 points, the estimation of the ground responses at the grid points are interpolated through Kriging analyses (ArcGIS 2004) in which the ordinary Kriging method is adopted.

The ground strain at each mesh is analyzed by the following procedure:

(1) To obtain the maximum displacement at each site.

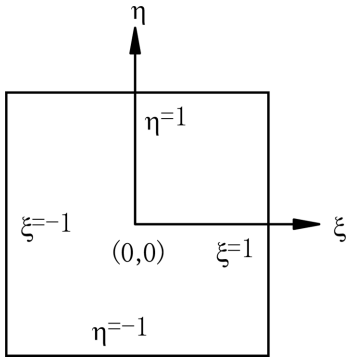

Fig. 12 The mesh coordinate system

(2) To estimate the maximum displacement at each grid of the meshes.
(3) To calculate the ground strain at each mesh by the following formula.

$$\begin{pmatrix} \varepsilon_x \\ \varepsilon_y \\ \gamma_{xy} \end{pmatrix} = \frac{1}{2ab} \begin{bmatrix} b(1+\eta) & -b(1+\eta) & -b(1-\eta) & b(1-\eta) & 0 & 0 & 0 & 0 \\ 0 & 0 & 0 & 0 & a(1+\xi) & a(1-\xi) & -a(1-\xi) & -a(1+\xi) \\ a(1+\xi) & a(1-\xi) & -a(1-\xi) & -a(1+\xi) & b(1+\eta) & -b(1+\eta) & -b(1-\eta) & b(1-\eta) \end{bmatrix} \begin{pmatrix} u_1 \\ u_2 \\ u_3 \\ u_4 \\ v_1 \\ v_2 \\ v_3 \\ v_4 \end{pmatrix} \tag{45}$$

where a, b are the lengths of a mesh, and ξ, η are the normalized coordinate components as shown in Fig. 12. ε_x, ε_y, γ_{xy} are strain components of a mesh, while u_i, v_i are displacement components at the i-th grid of a mesh.

(4) To make the representative value of the ground strain at each mesh by

$$\varepsilon_G = \frac{1}{2}(\varepsilon_x + \varepsilon_y) + \left\{ \gamma_{xy}^2 + \frac{1}{4}(\varepsilon_x - \varepsilon_y) \right\}^{1/2} \tag{46}$$

5.3 Phase velocity derived from the observed data

The rectangular portion near the fault zone (black thick line) is selected for the accurate data analysis, while the other portions are roughly estimated. Applying the ground response velocity at 441 sites to Kriging analysis, the particle velocity distribution is shown in Fig. 14.

Based on Eqs. (45) and (46), the ground strain distribution are calculated as shown in Fig. 15.

Once the particle velocity $\dot{u}_{\max}$ and the ground strain ε_G at each mesh are selected from Figs. 15 and 16, the phase velocity V for that mesh can be obtained by the following equation.

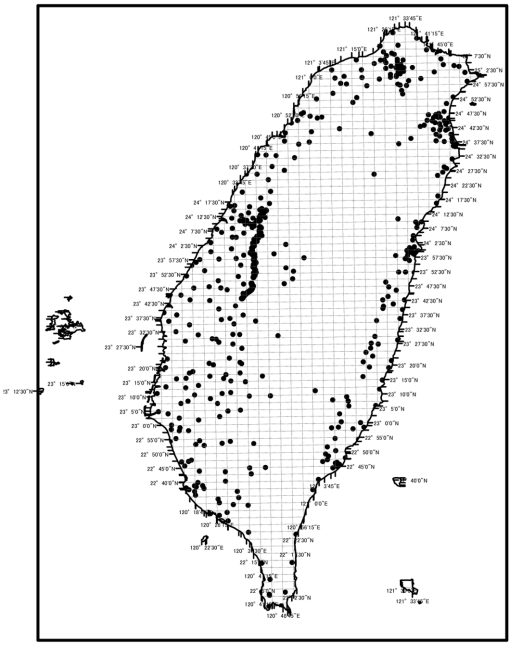

Fig. 13 The observation sites

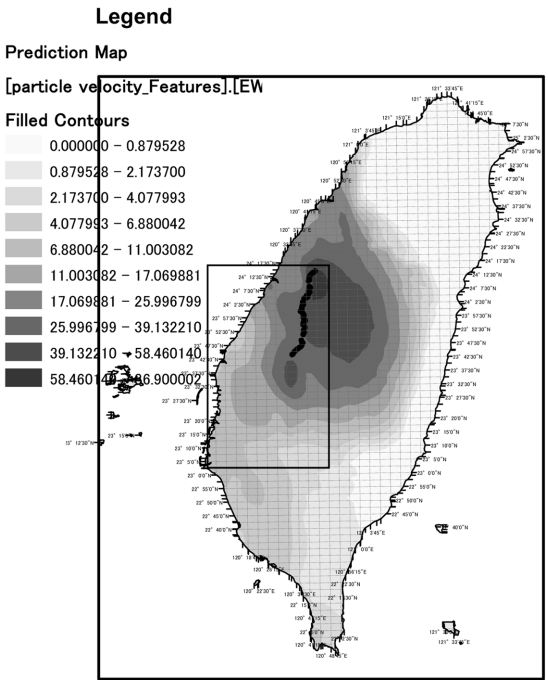

Fig. 14 The particle velocity (NS comp.)

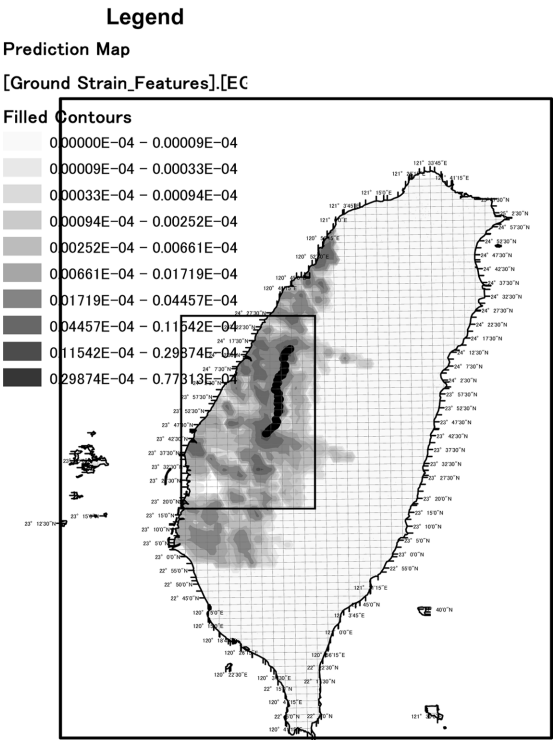

Fig. 15 The ground strain distribution

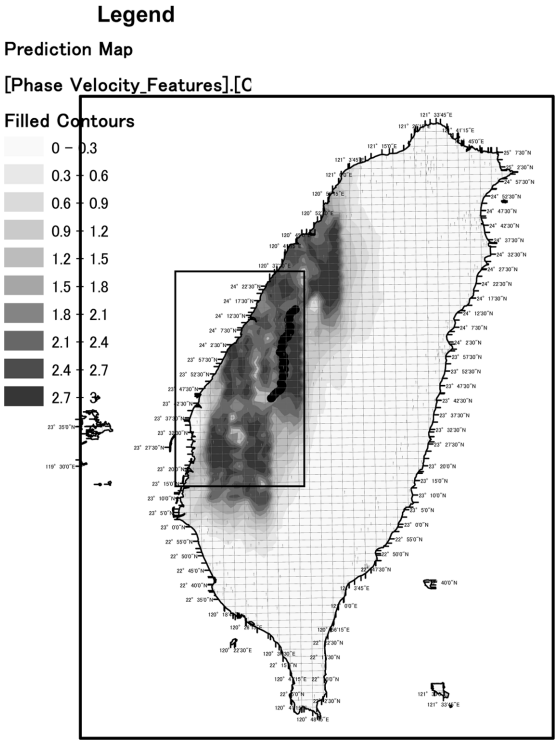

Fig. 16 The phase velocity distribution

$$V \approx \frac{\dot{u}_{\max}}{\varepsilon_G} \tag{47}$$

The phase velocity given in Fig. 16 shows around the values of 300 m/sec to 3 km/sec. Almost large portion of the phase velocity is between 1 km/sec to 2 km/sec, while some local area shows lower velocity, especially in the south western area from the south end of the fault zone.

In this analysis, the geo-technical conditions of the whole area are not taken into consideration, although the spatial variation of the phase velocity will be caused by the varieties of the geo-technical conditions.

In the previous section, the phase velocities of surface wave models are calculated in Fig. 6, where the maximum phase velocity is assumed to be 800 m/sec. The observation result, however, shown in Fig. 16 suggests that the maximum phase velocity for such a design curve should be a larger value of 1 km/sec to 2 km/sec than 800 m/sec.

6. Conclusions

A theoretical approach based on the horizontally propagating wave models is developed in order to resolve the difficulty in evaluating the structural strains of buried pipelines conveying different materials. The structural strains of buried pipelines are not always identical even under the same design condition, since the current design guidelines in Japan are diverse in the seismic ground strain estimates.

Investigations were made for four different wave models which are surface wave models of Rayleigh and Love waves, a SH wave model with spatial variation and a SH wave model with a phase delay propagating in the baserock.

Numerical results show that the surface wave model can produce larger ground strain than that of current seismic design level especially in the range of a typical period exceeding 1.0 second, while the SH wave model shows small strains less than that of current design level. The spatial variation with the relative interval less than 300 m can produce relatively large ground strain.

Spatially distributed ground motion are observed at 441 measurement points by Central Weather Bureau (CWB) of Taiwan in the 1991 Chi-Chi. In this study those data are analyzed to estimate the phase velocity at the ground surface located near the fault zone of this earthquake.

It can be noted that the phase velocity obtained by the observed data shows a larger value of 1 km/sec to 2 km/sec than 800 m/sec which is the design phase velocity of the ground in the longer typical period.

References

ArcGIS (2004), *Geostatistical Analyst*, ArcView Ver.8, ESRI Japan.

Brune, J.N. (1970), "Tectonic stress and the spectra of seismic shear waves from earthquakes", *J. Geophysical Res.*, **75**, 4997-5009.

Di Paola, M. and Zingales, M. (2000), "Digital simulation of multivariate earthquake ground motions", *Earthq. Eng. Struct. Dyn.*, **29**, 1011-1027.

Harada, T., Tanaka, T. and Tamura, Y. (1995), "Digital simulation of earthquake ground motions using a seismological model", JSCE, No.507/I-30, 209-217.

Haskell, N.A. (1953), "The dispersion of surface waves on multilayered media", *Bulletin of Seismological Society of America*, **43**(17).
Hong, H. and Zhang, S-R. (1999), "Spatial ground motion effect on relative displacement of adjacent building structures", *Earthq. Eng. Struct. Dyn.*, **28**, 333-349.
Irikura, K. (1986), "Prediction of strong accelerations motions using empirical Green's function", *Proc. of 7th Japan Earthquake Engineering Symposium*, 151-156.
Japan Gas Association (2000), *Seismic Design Guideline of High-pressure Gas Pipelines*, Japan Gas Association.
Japan Water Works Association (1998), *Seismic Design Guideline of Water Works Facilities*, Japan Water Works Association.
Kamae, K., Irikura, K. and Fukuchi, Y. (1991), "Prediction of strong motion at the great earthquake based on the scaling criterion", *J. Japan Society of Architectural Eng.*, No.430, 1-9 (in Japanese).
Kramer, S.L. (1996), *Geotecnical Earthquake Engineering*, Prentice Hall, U.S.A., 156-174.
Lee, W.H.K., Shin, T.C., Kuo, K.W., Chen, K.C. and Wu, C.F. (2001), "CWB free-field strong-motion data from the 21 September Chi-Chi, Taiwan Earthquake", *Bulletin of the Seismological Society of America*, **91**(5), 1370-1376.
Loh, C.H. and Yeh, Y.T. (1988), "Spatial variation and stochastic modeling of seismic differential ground movement", *Earthq. Eng. Struct. Dyn.*, **16**(4).
Ogawa, Y. and Koike, T. (2001), "Structural design of buried pipelines for severe earthquakes", *Soil Dyn. Earthq. Eng.*, **21**, 199-209.
Research Group of Theoretical Earthquake Ground Motion (1994), *Earthquake Ground Motion*, edited by M. Izumi, Kajima Publishing Co. Ltd., p.124.
Shinozuka, M., Kameda, H. and Koike, T. (1983), "Ground strain estimation for seismic risk analysis", ASCE, **109**(1), 175-191.
Vanmarcke, E.H. (1972), "Properties of spectral moments with applications to random vibration", ASCE, **92**, No.EM2, 425-446.

Appendix

$$\frac{1}{\eta} = \frac{\dot{u}_0}{\dot{w}_0} = \frac{J_{22}-J_{12}}{J_{11}-J_{21}} = \frac{J_{42}-J_{32}}{J_{31}-J_{41}}, \qquad J = E_m^{-1}\prod_{j=1}^{m-1}\{D_j(d_j)\,E_j^{-1}\}$$

$$E_m = \begin{bmatrix} -\left(\frac{v_{pm}}{V}\right)^2 & 0 & -\Gamma_m r_{\beta m} & 0 \\ 0 & -\left(\frac{v_{pm}}{V}\right)^2 r_{\alpha m} & 0 & \Gamma_m \\ -\rho_m v_{pm}^2(\Gamma_m - 1) & 0 & -\rho_m V^2 \Gamma_m^2 r_{\beta m} & 0 \\ 0 & \rho_m v_{pm}^2 \Gamma_m r_{\alpha m} & 0 & -\rho_m V^2 \Gamma_m(\Gamma_m - 1) \end{bmatrix}$$

$$D_m(z_m) = \begin{bmatrix} -\left(\frac{v_{pm}}{V}\right)^2 \cos P_m & i\left(\frac{v_{pm}}{V}\right)^2 \sin P_m & -\Gamma_m r_{\alpha m}\cos Q_m & i\Gamma_m r_{\beta m}\sin Q_m \\ i\left(\frac{v_{pm}}{V}\right)^2 r_{\alpha m}\sin P_m & -\left(\frac{v_{pm}}{V}\right)^2 r_{\alpha m}\cos P_m & -i\Gamma_m \sin Q_m & \Gamma_m \cos Q_m \\ -\rho_m v_{pm}^2(\Gamma_m - 1)\cos P_m & i\rho_m v_{pm}^2(\Gamma_m - 1)\sin P_m & -\rho_m V^2 \Gamma_m^2 r_{\beta m}\cos Q_m & i\rho_m V^2 \Gamma_m^2 r_{\beta m}\sin Q_m \\ -i\rho_m v_{pm}^2 \Gamma_m r_{\alpha m}\sin P_m & \rho_m v_{pm}^2 \Gamma_m r_{\alpha m}\cos P_m & i\rho_m V^2 \Gamma_m(\Gamma_m - 1)\sin Q_m & -\rho_m V^2 \Gamma_m(\Gamma_m - 1)\cos Q_m \end{bmatrix}$$

$$v_{pm} = \sqrt{\frac{\lambda_m + 2\mu_m}{\rho_m}}, \quad v_{sm} = \sqrt{\frac{\mu_m}{\rho_m}}, \quad \Gamma_m = 2\left(\frac{v_{sm}}{V}\right)^2, \quad P_m = kr_{\alpha m} z_m, \quad Q_m = kr_{\beta m} z_m, \quad k = \frac{\omega}{V}$$

$$r_{\alpha m} = \sqrt{\left(\frac{V}{v_{pm}}\right)^2 - 1}; \quad V \geq v_{pm}; \quad r_{\beta m} = \sqrt{\left(\frac{V}{v_{sm}}\right)^2 - 1}; \quad V \geq v_{sm}$$

$$r_{\alpha m} = -i\sqrt{1 - \left(\frac{V}{v_{pm}}\right)^2}; \quad V < v_{pm}; \quad r_{\beta m} = -i\sqrt{1 - \left(\frac{V}{v_{sm}}\right)^2}; \quad V < v_{sm}$$

$S_m(z_m) = D_m(z_m)E_m^{-1}\prod_{j=1}^{m-1}\{D_j(d_j)E_j^{-1}\}$, S_{m11} and S_{m12} are the (1-1) and (1-2) elements of $S_m(z_m)$